Influence of longitudinal and lateral confinements on excitons in cylindrical quantum dots of semiconductors

S. Le Goff and B. Stébé
Université de Metz et Ecole Supérieure d'Electricité, Laboratoire d'Optoélectronique et de Microélectronique, 1 Boulevard Arago, 57078 Metz CEDEX 3, France
(Received 20 May 1992)

The ground-state energy of an exciton in a cylindrical quantum dot with finite potential barriers is calculated by the variation method within the envelope-function approximation. The computations are performed in the cases of infinite and finite band offsets. The limit of a strictly two-dimensional quantum disk is discussed. Our numerical results are particularized to the $GaAs/Ga_{1-x}Al_xAs$ system with $0.10 \leq x \leq 0.30$. In this case, the effect of the quantum confinement is the highest for dot dimensions near 50 Å.

I. INTRODUCTION

Recent progress[1] in submicrometer technology has made possible the fabrication of new types of semiconductor heterostructures whose characteristic dimensions (a few nanometers) become comparable to the de Broglie wavelengths of the free carriers. Consequently, the effects of the spatial quantum confinement become appreciable and restrict the electron and hole mobilities in two dimensions (quantum wells, superlattices) or one dimension (quantum wires). Recently, increasing attention has been focused on "zero-dimensional" (0D) nanometer-size structures by fabricating microcrystals and "quantum dots," also called "quantum boxes" or "quantum disks," where the ultimate quantum confinement effects confine the electrons and the holes in all three space dimensions. Their interest resides essentially in their nonlinear optical properties and the possibility to realize high-performance quantum dot lasers. Until recently, progress in making 0D nanometer-size structures has been almost entirely limited to colloidal solutions of II-VI microcrystallites or II-VI and I-VII crystals embedded in a glass or alkali halide matrix.[2,3] Since 1986, advances in material preparation, in particular molecular-beam epitaxy and the improvement of the lithographic techniques, have made possible the fabrication of quasi-0D quantum dots derived from $GaAs/Ga_{1-x}Al_xAs$ 2D heterostructures or similar systems.[4–15] They are typically a few hundred nanometers wide and a few nanometers thick, and can exhibit various shapes. Whereas the microcrystallites are approximately spherical, the quantum dots are better described by thin disks[6] or cylinders.[11,13] Because the quantum confinement increases highly the electron-hole Coulomb interaction, the "excitons" (i.e., confined electron-hole states) remain present at room temperature in both absorption and emission spectra. Therefore, many devices using excitonic transitions have been proposed. These effects are expected to be particularly important when the dimensions of the boxes become comparable to the exciton effective Bohr radius. Although many theoretical studies have been devoted[16–31] to excitonic states in spherical microcrystals, very few papers concern excitons in quantum dots. Up to now, two box shapes have been considered: square flat plates[32,33] and cylindrical[34] boxes. In these latter cases, infinite barriers have been used to confine the electron and the hole.

In this paper, we present the results of a variational calculation of the ground-state energy of an exciton in a cylindrical dot with finite electron and hole barriers. In Sec. II, we present the theoretical model used to describe the exciton in a cylindrical quantum box. In Sec. III, we first study the much simpler case of infinite potential barriers in order to discuss the validity of our wave function. In Sec. IV, we present the results obtained in the general case of finite barriers for the $GaAs/Ga_{1-x}Al_xAs$ system, and the conclusion is made in Sec. V.

II. THEORY

We consider an exciton in an isolated cylindrical semiconductor quantum box of radius R and height H (Fig. 1), embedded in another infinitely large semiconductor with a higher energy gap. We assume that the conduction- and valence-band offsets are weak enough so that the envelope-function approximation may be used in a two-band model. In the case of isotropic parabolic non-

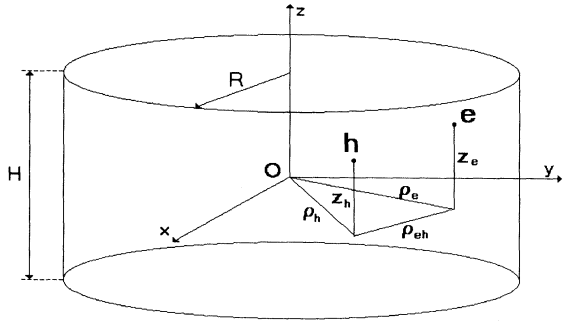

FIG. 1. Electron-hole pair in a cylindrical quantum dot. Definition of coordinates is given.

degenerated bands, the effective Hamiltonian then reads

$$H=-\frac{\hbar^2}{2m_e^*}\nabla_e^2-\frac{\hbar^2}{2m_h^*}\nabla_h^2-\frac{e^2}{\kappa|\mathbf{r}_e-\mathbf{r}_h|}+V_w^e(\mathbf{r}_e)+V_w^h(\mathbf{r}_h)\ , \quad (1)$$

where m_e^* and m_h^* denote the electron and hole effective masses. We assume that they are the same in the dot and in the outside materials. The dielectric constant κ, introduced in a quite phenomenologic way, regulates for possible polarization effects and is also supposed to be the same in the two materials. V_w^e and V_w^h are, respectively, the electron and the hole well potential arising from the band offsets:

$$V_w^i=V_i\theta(\rho_i-R)\theta(|z_i|-H/2)\quad (i=e,h)\ , \quad (2)$$

where V_e and V_h are the electron and hole barrier heights. $\theta(x)$ is the step function [$\theta(x)=1$ if $x>0$; $\theta(x)=0$ if $x<0$]. z_e and z_h are the electron and hole coordinates along the z axis, which we assume to be parallel to the cylinder axis, and ρ_e,ρ_h are the electron and hole coordinates in the plane perpendicular to the cylinder axis.

The energy E and the envelope wave function Ψ are obtained as solutions of the following effective-mass Schrödinger equation:

$$H\Psi=(\epsilon-\epsilon_g)\Psi=E\Psi\ , \quad (3)$$

where ϵ_g corresponds to the dot-material energy-gap discontinuity between the conduction and valence bands. We determine the ground-state solution of Eq. (3) by means of the variation method.

In order to choose the trial wave function, we examine first some limiting cases. The bulk 3D situation may be achieved when V_e and V_h vanish, or when R and H become very large, whether the values of the potential are finite or infinite. In this limit, the ground-state energy E_X^{3D} and wave function Ψ^{3D} are well known:

$$E_X^{3D}=-\frac{\mu e^4}{2\kappa^2\hbar^2}\ ,\quad \Psi^{3D}=\exp(-r/a_X^{3D})\ , \quad (4)$$

where $1/\mu=1/m_e^*+1/m_h^*$ and r denotes the electron-hole distance, while $a_X^{3D}=\kappa\hbar^2/\mu e^2$ stands for the 3D exciton Bohr radius.

In the case of a finite potential well, we get again the 3D exciton in the three limiting cases (i) $R\to 0$ and $H\to 0$; (ii) $R\to\infty$ and $H\to 0$; (iii) $R\to 0$ and $H\to\infty$. If H remains finite, we get a 1D quantum-well (QW) whose confinement direction is parallel to the z axis in the two cases (i) $R\to 0$, (ii) $R\to\infty$. On the other hand, if R remains finite, we get a quantum-well wire (QWW) directed along the z axis in the two cases (i) $H\to 0$, (ii) $H\to\infty$.

In the case of an infinite potential well, the 2D exciton is encountered if $R\to\infty$ and $H\to 0$. The corresponding energy is $E_X^{2D}=4E_X^{3D}$, while the wave function is $\Psi^{2D}=\exp(-r/a_X^{2D})$, with $a_X^{2D}=a_X^{3D}/2$. If H has a finite constant value, the QW is obtained only if $R\to\infty$. On the other hand, if R remains finite, we get the QWW only if $H\to\infty$. The case of the quantum disk ($H=0$) will be discussed later. In the limit of ultrasmall dots, the effect of the quantum confinement becomes much larger than that of the Coulombic electron-hole interaction. The total exciton energy may then be approximated by the sum of that of the noncorrelated confined electron and hole. The corresponding ground-state wave function then reads

$$\Psi^0=f_e(\rho_e)g_e(z_e)f_h(\rho_h)g_h(z_h)\ , \quad (5)$$

with

$$f_i(\rho)=J_0(\theta_0\rho/R)\ ,\quad g_i(z)=\cos(\pi z/H)\quad (i=e,h)\ . \quad (6)$$

J_0 is the Bessel function of zero order; $\theta_0=2.404\,825\,557\,7$ is its first zero.[35] The energy of this ground state is the sum of the energies of the confined electron and hole:

$$E_e+E_h=(\hbar^2/2m_e^*+\hbar^2/2m_h^*)[(\theta_0/R)^2+(\pi/H)^2]\ . \quad (7)$$

We remark that the wave functions of confined electrons or holes are identical. Indeed, they do not depend on their effective masses. However, it appears that the energy sum (7) depends on the reduced mass μ. In the following, we use the atomic units a_X^{3D} for length and $|E_X^{3D}|$ for energy. In these units, the noncorrelated pair energy becomes independent of the effective masses:

$$E_e+E_h=(\theta_0/R)^2+(\pi/H)^2\ . \quad (8)$$

It must be stressed that this conclusion holds only in the case of infinite potential wells. It appears that, owing to the quantum confinement, a strong singularity arises for ultrasmall boxes in the case of infinite potential wells.

Generally speaking, we may define the exciton wave function using the six independent coordinates (ρ_i,ϕ_i,z_i), where ϕ_i is the angular coordinate of the particle i ($i=e,h$). However, in the ground state, the system is invariant under every rotation about the z axis, so that the angular dependence may be reduced to $\Phi=\phi_e-\phi_h$, varying between $-\pi$ and π. This latter may also be described by the in-plane electron-hole distance ρ_{eh}, although two opposite values of Φ correspond to a given value of ρ_{eh}. We therefore choose the following trial wave function:

$$\Phi_X=F_e(\rho_e,z_e)F_h(\rho_h,z_h)F_{eh}(\rho_{eh},|z_e-z_h|)\ , \quad (9)$$

where the product function F_eF_h describes the confinement of the uncorrelated electron-hole pair. It reduces to the expression (5) in the case of infinite potential wells. In Sec. IV, we shall discuss its expression in the case of infinite potential wells. F_{eh} describes the internal motion of the exciton. For large R and H, it reduces to its 3D limit (4). In the other cases, it may be approximated by a screened variational function. The following function has been used[34] recently:

$$F_{eh}(\rho_{eh},|z_e-z_h|)=\exp\{-\alpha[\rho_{eh}^2+(z_e-z_h)^2]^{1/2}\}\ . \quad (10)$$

In this approximation, it depends only on the electron-hole distance, and does not take into account the anisotropy of the dot, which may be important for different R and H values, though it is expected to give accurate re-

sults in the limits of weak quantum confinement ($R \to \infty$, $H \to \infty$). However, because such a function is nonseparable in ρ_{eh} and z_e, z_h, it gives rise to rather complicated calculations because of the occurrence of fourfold integrals. Therefore, we choose the following more simple separable function:

$$F_{eh}(\rho_{eh}, |z_e - z_h|) = \exp(-\alpha\rho_{eh}) \exp[-\gamma(z_e - z_h)^2] \ . \tag{11}$$

Two different variational parameters α and γ are introduced in order to take into account the possible anisotropy of the dot. In this form, our wave function gives rise to a simpler numerical computation because of the occurrence of only threefold integrals. Though the proper hydrogenlike 3D exciton wave function is not reproduced in the 3D limit, this function is expected to be a good approximation in the limit of strong quantum confinement, and in the 2D limit. Its behavior is better when $H/R < 1$. We made this choice because it is much easier to produce a very small height than a very small radius.

Finally, the ground-state wave function and the energy are determined by minimizing the mean energy:

$$\langle E(\alpha,\gamma) \rangle = \langle \Psi_X | H | \Psi_X \rangle / \langle \Psi_X | \Psi_X \rangle \ , \tag{12}$$

for all variations of the two parameters α and γ. In order to study the influence of the Coulombic correlation, we define also the correlating energy

$$\langle W \rangle = \langle E \rangle - E_e - E_h \ . \tag{13}$$

III. INFINITE QUANTUM-WELL MODEL

A. Variational calculation of the binding energy

We first study the much simpler case of infinite potential barriers, in order to check whether our wave function describes correctly the above discussed limiting cases. In our system of atomic units, the effective Hamiltonian reads

$$\begin{aligned} H = &-\frac{1}{1+\sigma}\left[\frac{\partial^2}{\partial\rho_e^2}+\frac{1}{\rho_e}\frac{\partial}{\partial\rho_e}+\frac{\rho_{eh}^2+\rho_e^2-\rho_h^2}{\rho_e\rho_{eh}}\frac{\partial^2}{\partial\rho_e\partial\rho_{eh}}+\frac{\partial^2}{\partial z_e^2}\right] \\ &-\frac{\sigma}{1+\sigma}\left[\frac{\partial^2}{\partial\rho_h^2}+\frac{1}{\rho_h}\frac{\partial}{\partial\rho_h}+\frac{\rho_{eh}^2+\rho_h^2-\rho_e^2}{\rho_h\rho_{eh}}\frac{\partial^2}{\partial\rho_h\partial\rho_{eh}}+\frac{\partial^2}{\partial z_h^2}\right] \\ &-\left[\frac{\partial^2}{\partial\rho_{eh}^2}+\frac{1}{\rho_{eh}}\frac{\partial}{\partial\rho_{eh}}\right]-\frac{2}{[\rho_{eh}^2+(z_e-z_h)^2]^{1/2}}+V_w^e(\rho_e,z_e)+V_w^h(\rho_h,z_h) \ , \end{aligned} \tag{14}$$

where we have introduced the effective-mass ratio $\sigma = m_e^*/m_h^*$. The mean energy (12) is then given by

$$\begin{aligned} \langle E(\alpha,\gamma) \rangle = &\left[\frac{\theta_0}{R}\right]^2+\left[\frac{\pi}{H}\right]^2-\alpha^2+\alpha\frac{P_3(\alpha,R)}{P_1(\alpha,R)}-\frac{\alpha}{1+\sigma}\frac{P_4(\alpha,R)+\sigma P_5(\alpha,R)}{P_1(\alpha,R)}+2\gamma \\ &-4\gamma^2\frac{Z_2(\gamma,H)}{Z_1(\gamma,H)}+\frac{4\gamma}{1+\sigma}\frac{Z_3(\gamma,H)+\sigma Z_4(\gamma,H)}{Z_1(\gamma,H)}+\langle V_{\text{Coul}} \rangle \ . \end{aligned} \tag{15}$$

The integrals P_i and Z_i are defined by

$$P_i = 8\pi\int_0^\infty d\rho_e\int_0^\infty d\rho_h\int_{|\rho_e-\rho_h|}^{\rho_e+\rho_h}\frac{F_i(\rho_e,\rho_h,\rho_{eh})\rho_e\rho_h\rho_{eh}\,d\rho_{eh}}{\{[(\rho_e+\rho_h)^2-\rho_{eh}^2][\rho_{eh}^2-(\rho_e-\rho_h)^2]\}^{1/2}} \ , \tag{16}$$

$$\begin{aligned} F_1(\rho_e,\rho_h,\rho_{eh}) &= [f_e(\rho_e)f_h(\rho_h)\exp(-\alpha\rho_{eh})]^2 \ , \\ F_3(\rho_e,\rho_h,\rho_{eh}) &= \frac{1}{\rho_{eh}}F_1(\rho_e,\rho_h,\rho_{eh}) \ , \\ F_4(\rho_e,\rho_h,\rho_{eh}) &= -\frac{\rho_{eh}^2+\rho_e^2-\rho_h^2}{\rho_e\rho_{eh}}f_e(\rho_e)f_e'(\rho_e) \\ &\quad\times[f_h(\rho_h)\exp(-\alpha\rho_{eh})]^2 \ , \\ F_5(\rho_e,\rho_h,\rho_{eh}) &= -\frac{\rho_{eh}^2+\rho_h^2-\rho_e^2}{\rho_h\rho_{eh}}f_h(\rho_h)f_h'(\rho_h) \\ &\quad\times[f_e(\rho_e)\exp(-\alpha\rho_{eh})]^2 \ ; \end{aligned} \tag{17}$$

and

$$Z_i = \int_{-\infty}^{\infty}dz_e\int_{-\infty}^{\infty}dz_h\,G_i(z_e,z_h) \ , \tag{18}$$

with

$$\begin{aligned} G_1(z_e,z_h) &= \{g_e(z_e)g_h(z_h)\exp[-\gamma(z_e-z_h)^2]\}^2 \ , \\ G_2(z_e,z_h) &= (z_e-z_h)^2G_1(z_e,z_h) \ , \\ G_3(z_e,z_h) &= (z_e-z_h)g_e(z_e)g_e'(z_e) \\ &\quad\times\{g_h(z_h)\exp[-\gamma(z_e-z_h)^2]\}^2 \ , \\ G_4(z_e,z_h) &= (z_h-z_e)g_h(z_h)g_h'(z_h) \\ &\quad\times\{g_e(z_e)\exp[-\gamma(z_e-z_h)^2]\}^2 \ . \end{aligned} \tag{19}$$

The P_i integrals will be computed numerically. In the case of the Z_i integrals, the integration over $z \equiv (z_e + z_h)/2$ may be performed analytically, while the remaining integration over $\zeta \equiv z_e - z_h$ will also be computed numerically.

We remark that it is only the case of infinite potential barriers that the uncorrelated functions (6) are the same for both the electron and the hole. Thus $F_4(\rho_e,\rho_h,\rho_{eh}) = F_5(\rho_h,\rho_e,\rho_{eh})$ and $G_3(z_e,z_h) = G_4(z_h,z_e)$. Because the integrations over the electron and hole coordinates may be inverted, we get

$$P_4(\alpha,R) = P_5(\alpha,R) , \quad Z_3(\gamma,H) = Z_4(\gamma,H) . \tag{20}$$

Thus, although the effective-mass ratio σ appears in the Hamiltonian, the energy does not depend on σ. However, it must be stressed that this property does not hold in the model of finite potential barriers. In the following, we discuss first the 2D limit, corresponding to the special case of a quantum disk, before we discuss our method of resolution in the general case.

B. Special case of the quantum disk

In the quantum disk limit ($H \to 0$), the z-axis coordinates z_e and z_h vanish, so that the wave function reduces to

$$\Psi_X = J_0(\theta_0 \rho_e / R) J_0(\theta_0 \rho_h / R) \exp(-\alpha \rho_{eh}) . \tag{21}$$

The mean value of the Coulombic energy then reads

$$\langle V_{\text{Coul}} \rangle = -2 P_3(\alpha,R)/P_1(\alpha,R) . \tag{22}$$

The mean energy (15) takes the simpler expression

$$\langle E(\alpha) \rangle = \left[\frac{\theta_0}{R} \right]^2 - \alpha^2 + (\alpha - 2) \frac{P_3(\alpha,R)}{P_1(\alpha,R)} - \alpha \frac{P_4(\alpha,R)}{P_1(\alpha,R)} . \tag{23}$$

In Fig. 2, the total energy $\langle E \rangle$, the correlation energy $\langle W \rangle$, the noncorrelated particle energy $E_e + E_h$, the Coulombic potential energy $\langle V \rangle$, and the kinetic energy are drawn against the radius of the disk. For large values of R, these curves show that we obtain the expected behavior. Indeed, we get the correct limiting values: $\langle E \rangle \to -4$ a.u., $\langle W \rangle \to -4$ a.u., $E_e + E_h \to 0$, $\langle V \rangle \to -8$ a.u., $\langle E \rangle \to +4$ a.u. The variational parameter α tends also to the theoretical limit $1/a_X^{2D} = 2$ a.u. for large values of R, as will be shown in Fig. 8. For very small values of R, it may be shown that the optimal value of α tends to 1.071 a.u., about twice the value (0.4980 a.u.) that has been obtained[23] using an analog wave function in the case of a quantum sphere with an infinite potential barrier. This difference is due to the influence of the geometrical confinement, because the electron-hole correlation is higher in the 2D case compared to the 3D case. In this limit, we get the following expression for the mean energy:

$$\langle E(\alpha, R \to 0) \rangle \simeq \theta_0^2 / R^2 - 5.189/R - 1.146 \text{ a.u.} \tag{24}$$

We can see that the electron-hole pair energy $E_e + E_h = \theta_0^2 / R^2$ becomes much higher than the absolute value of the correlation energy, although this latter goes to infinity. It is only in this sense that we can speak of an "uncorrelated electron-hole pair limit," because the Coulombic energy becomes infinite.

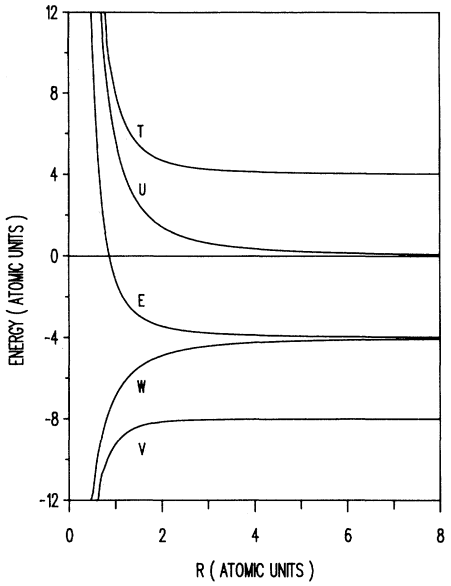

FIG. 2. Total energy E, uncorrelated pair energy $U = E_e + E_h$, kinetic energy T, Coulombic potential energy V, and correlation energy $W = E - U$ drawn vs the radius for an exciton in a quantum disk with infinite potential-well barriers.

C. General case of the quantum cylinder

When R and H remain finite and nonzero, the expectation value of the Coulombic energy reads

$$\langle V_{\text{Coul}} \rangle = -2 \int_{-\infty}^{\infty} dz_e \int_{-\infty}^{\infty} dz_h G_1(z_e,z_h) P_c(\alpha,R,z_e - z_h) , \tag{25}$$

where P_c is analog to the P_i integrals (16). Here

$$F_c(\rho_e,\rho_h,\rho_{eh}) = F_1(\rho_e,\rho_h,\rho_{eh}) / [\rho_{eh}^2 + (z_e - z_h)^2]^{1/2} . \tag{26}$$

In order to simplify the numerical computations, we determine $\langle V_{\text{Coul}} \rangle$ using the following approximate expression for the P_c integrals:

$$\phi_\alpha(z_e - z_h) = \frac{a}{b + |z_e - z_h|} , \tag{27}$$

where the constants a and b are chosen so that exact values of $\langle V_{\text{Coul}} \rangle$ are obtained in the limits $|z_e - z_h| \to 0$ and $|z_e - z_h| \to \infty$. For large values of $|z_e - z_h|$, $\phi_\alpha(z_e - z_h) \simeq a/(|z_e - z_h|)$, while $P_c(\alpha,R,z_e - z_h) \simeq P_1(\alpha,R)/(|z_e - z_h|)$; thus, we get $a = P_1(\alpha,R)$. On the other hand, if $|z_e - z_h|$ is small, $\phi_\alpha(z_e - z_h) \simeq a/b$, while $P_c(\alpha,R,z_e - z_h) \simeq P_3(\alpha,R)$; thus, $a/b = P_3(\alpha,R)$. So the approximate expression of $\langle V_{\text{Coul}} \rangle$ is given by

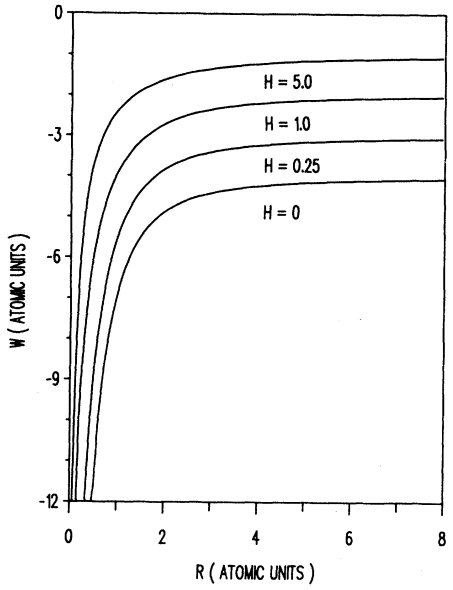

FIG. 3. Correlation energy W of an exciton confined in a quantum cylinder with infinite barriers, plotted against R for $H=0$ (disk limit) and three other values of the height H.

$$\langle V_{\text{Coul}} \rangle = -2Z_c(\alpha,R,\gamma,H)/Z_1(\gamma,H) , \tag{28}$$

where Z_c is analog to the Z_i integrals (18), with

$$G_c(H,R,\alpha,\gamma,z_e,z_h)=\frac{G_1(z_e,z_h)}{\dfrac{P_1(\alpha,R)}{P_3(\alpha,R)}+|z_e-z_h|} . \tag{29}$$

In Fig. 3, we have reported the variation of the correlation energy against R for different values of H. It appears, as expected, that for all values of H, $W\to-\infty$ when $R\to 0$. For fixed R values, W is an increasing function of H, with the limit $H=0$ corresponding to the lowest correlation energy. When $R\to\infty$, we get the QW limit. In all cases, the quantum confinement increases the effect of the Coulomb correlation. In Fig. 4, we compare the variations, against R, of the variational parameters α and γ for a fixed value of H. In particular, we remark that for very low R values, α becomes very small while γ becomes very large. This means that in this limit, the z correlation becomes much higher than the in-plane correlation. This result cannot be shown using the previously used[34] isotropic electron-hole correlation function (10).

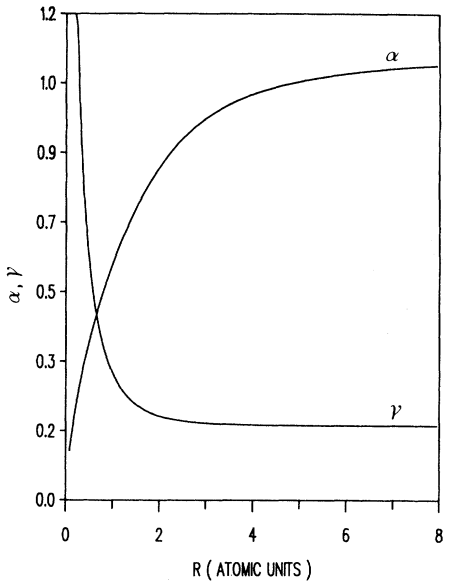

FIG. 4. Variational parameters α and γ, expressed in atomic units, plotted against the radius (R) of the quantum cylinder in the case of an infinite well for $H=1$ a.u.

IV. FINITE QUANTUM-WELL MODEL

For very small dot sizes, the infinite-well model fails strongly because tunneling effects become very important. In the following discussion, we attempt to take into account the effect due to finite band offsets.

A. Noncorrelated electron and hole ground states

In the finite barrier model, the problem is much more difficult, because the well potential (2) cannot be written as a sum like $V^i_{wp}(\rho_i)+V^i_{wz}(z_i)$ of an in-plane potential and a z-axis potential, so that the product $f_i(\rho_i)g_i(z_i)$ is no longer an exact solution of the single-particle Schrödinger equation.

Let us first investigate the in-plane motion. In our atomic units, the 2D effective-mass Schrödinger equation reads

$$-\tau_i\nabla_i^2 f_i(\rho_i)+V^i_{wp}(\rho_i)f_i(\rho_i)=E_i f_i(\rho_i) , \tag{30}$$

with

$$\tau_e=\frac{1}{1+\sigma} , \quad \tau_h=\frac{\sigma}{1+\sigma} , \quad V^i_{wp}(\rho_i)=V_i\theta(\rho_i-R) . \tag{31}$$

This equation can be solved analytically. The ground-state wave functions read

$$f_i(\rho_i)=\begin{cases} J_0(\theta_i\rho_i/R) & \text{if } \rho_i<R , \\ A_iK_0(\beta_i\rho_i) & \text{if } \rho_i>R , \end{cases} \tag{32}$$

with $\beta_i=[V_i/\tau_i-(\theta_i/R)^2]^{1/2}$. J_0 and K_0 are, respectively, the zero-order Bessel function and the modified Bessel function. θ_i and A_i are constants determined by the boundary conditions at $\rho_i=R$:

$$\begin{aligned} &A_i=J_0(\theta_i)/K_0(\beta_iR) , \\ &\theta_iJ_1(\theta_i)/J_0(\theta_i)=\beta_iRK_1(\beta_iR)/K_0(\beta_iR) . \end{aligned} \tag{33}$$

The corresponding energy reads

$$E_{ip}=\tau_i(\theta_i/R)^2 . \tag{34}$$

For the z-axis motion, the ground-state solution of the Schrödinger equation becomes

$$g_i(z_i)=\begin{cases} \cos(\pi_iz_i/H) & \text{if } |z_i|<H/2 , \\ B_i\exp(-k_i|z_i|) & \text{if } |z_i|>H/2 , \end{cases} \tag{35}$$

with $k_i=[V_i/\tau_i-(\pi_i/H)^2]^{1/2}$. π_i and B_i are constants

determined by the boundary conditions at $z_i = H/2$:

$$B_i = \cos(\pi_i/2)/\exp(-k_i H/2) ,$$
$$\tan(\pi_i/2) = k_i H/\pi_i . \tag{36}$$

In this case, we get the energy

$$E_{iz} = \tau_i(\pi_i/H)^2 . \tag{37}$$

In the following discussion, we apply our results to the case of $GaAs/Ga_{1-x}Al_xAs$. We use the following material data:[36] $m_e^*/m_0 = 0.0665$ for the electron mass, and $m_{hh}^*/m_0 = 0.34$ and $m_{lh}^*/m_0 = 0.094$ for the heavy- and light-hole masses, respectively. The band offsets are given by $V_e = Q_e \epsilon_g$ and $V_h = Q_h \epsilon_g$, where $Q_e = 0.57 = 1 - Q_h$. Further, we assume that the band gap ϵ_g and the aluminum percentage x are related by[37] $\epsilon_g = 1.155x + 0.37x^2$ eV. Using the value[38] $\kappa = 12.5$ for the dielectric constant, we get $a_X^{3D} = 118.96$ Å and 169.89 Å for the heavy- and light-hole atomic units of length, and $|E_X^{3D}| = 4.84$ meV and 3.39 meV for the heavy- and light-hole units of energy. Figure 5 shows the variations of θ_i and π_i against R and H, respectively. It can be seen that, for large values of R, θ_i tends to θ_0, which is also the infinite-well limit. Similarly, for large values of H, π_i tends to the infinite-well limit π. The wave functions for the finite and infinite models are thus quite identical for large dots. They differ in the strong confinement case, which corresponds to dot dimensions smaller than the 3D exciton radius.

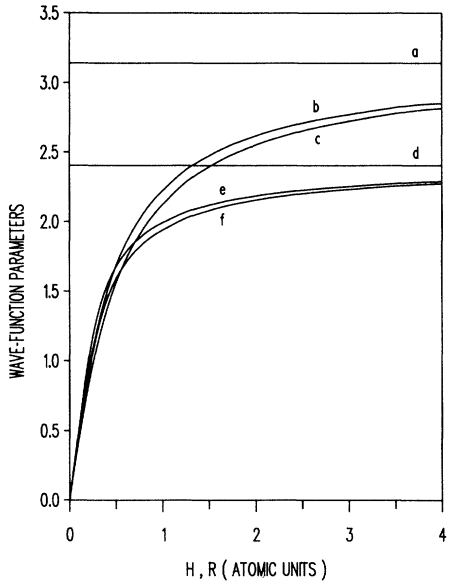

FIG. 5. Variations against H of the parameters π_e (b) and π_h (c) defining the one-particle wave functions in the case of a finite well with $x = 0.15$ and $\sigma = 0.196$ (heavy hole). The straight line (a) corresponds to their limit π when $H \to \infty$, which is also their constant value in the case of an infinite potential well. The curves (d), (e), and (f) show the variations of the analog parameters θ_e (e) and θ_h (f) as functions of R. The straight line (d) corresponds to their limit $\theta_0 = 2.405$ when $R \to \infty$, which is also their constant value in the case of an infinite potential well.

For the 3D motion, the product $f_i(\rho_i)g_i(z_i)$ is no longer a solution of the Schrödinger effective-mass equation, but is expected to be a better approximation of the wave function for small values of R and H. Let us rewrite the 3D confinement potential:

$$V_w^i(\mathbf{r}_i) = V_{wp}^i(\rho_i) + V_{wz}^i(z_i) - \delta V_i(\rho_i, z_i) , \tag{38}$$

where δV_i is a correction term defined by

$$\delta V_i = \begin{cases} 0 & \text{if } \rho_i < R , \quad |z_i| < H/2 , \\ V_i & \text{otherwise} . \end{cases} \tag{39}$$

Looking at $-\delta V_i$ as a perturbation potential, the ground-state single-particle energy can be approximated by

$$E_i = E_{ip} + E_{iz} - \langle \delta V_i \rangle$$
$$= \tau_i[(\theta_i/R)^2 + (\pi_i/H)^2]$$
$$- \langle f_i g_i | \delta V_i | f_i g_i \rangle / \langle f_i g_i | f_i g_i \rangle . \tag{40}$$

For large dots, the correction term due to $-\delta V_i$ vanishes. In this case, the expression (40) reduces to the infinite-well single-particle expression.

B. Special case of the quantum disk

In the quantum disk limit ($H \to 0$), the z-axis coordinates z_e and z_h vanish. We choose the following wave function:

$$\Psi_X = f_e(\rho_e) f_h(\rho_h) \exp(-\alpha \rho_{eh}) , \tag{41}$$

where f_e and f_h are the exact ground-state wave functions (32) of the uncorrelated particles in this geometry. The mean energy (15) becomes

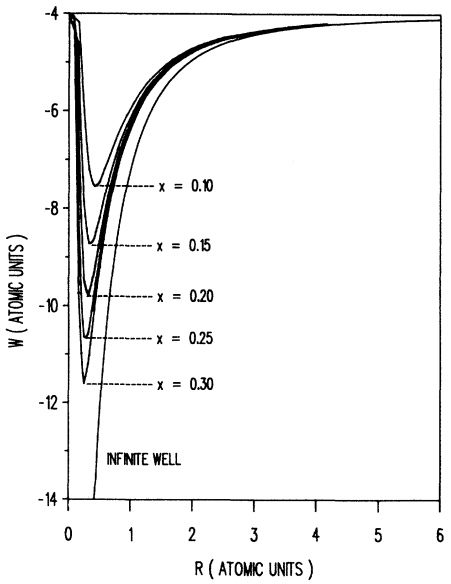

FIG. 6. Correlation energy of an exciton in a disk, drawn against R for different values of x, for $\sigma = 0.196$ and in the infinite-well approximation.

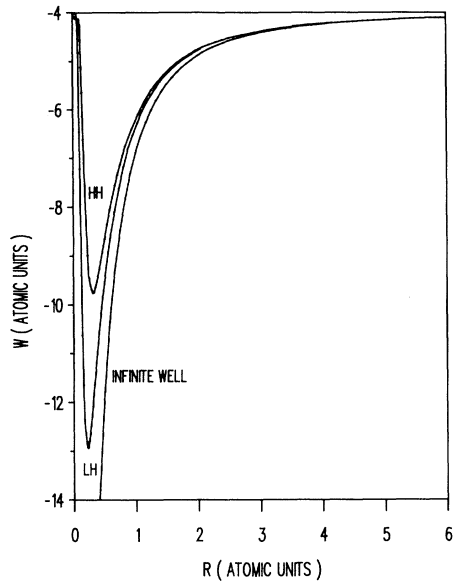

FIG. 7. Correlation energy (W) of an exciton in a disk, drawn against R for $\sigma=0.196$ (heavy hole) and for $\sigma=0.707$ (light hole) in the finite-well ($x=0.2$) and in the infinite-well approximation. The use of our atomic units ($|E_X^{3D}|$ for the energy and a_X^{3D} for the length) has the consequence that, in the infinite-well approximation, different σ values lead to the same curve, despite the values of these units being different for different values of σ.

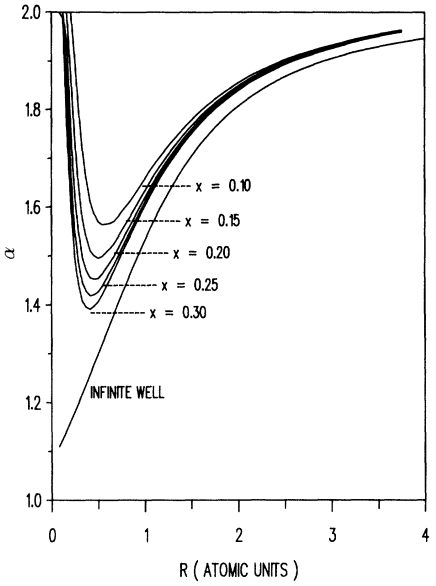

FIG. 8. Variational parameter α in atomic units of wave function of an exciton in a disk, drawn against R for different values of x and in the infinite-well approximation.

$$\langle E(\alpha)\rangle=\frac{1}{1+\sigma}[(\theta_e/R)^2+\sigma(\theta_h/R)^2]-\alpha^2+(\alpha-2)\frac{P_3(\alpha,R)}{P_1(\alpha,R)}-\frac{\alpha}{1+\sigma}\frac{P_4(\alpha,R)+\sigma P_5(\alpha,R)}{P_1(\alpha,R)}\ , \tag{42}$$

where P_i keeps the same meaning as in (16), with the new choice for f_e and f_h. Figures 6 and 7 show the variations of the correlation energy against R, while Fig. 8 reports the values of the variational parameter α.

C. General case of the quantum cylinder

In the finite-quantum-well model, we use a trial wave function (9) analogous to the infinite-well-model one. Here we choose

$$F_i(\rho_i,z_i)=f_i(\rho_i)g_i(z_i)\ ,\quad i=(e,h) \tag{43}$$

where f_i are the wave functions (32) and g_i the wave functions (35). There appear some new terms in the expectation value of the energy:

$$\langle E(\alpha,\gamma)\rangle=\frac{1}{1+\sigma}[(\theta_e/R)^2+\sigma(\theta_h/R)^2+(\pi_e/H)^2+\sigma(\pi_h/H)^2]-\alpha^2+\alpha\frac{P_3(\alpha,R)}{P_1(\alpha,R)}-\frac{\alpha}{1+\sigma}\frac{P_4(\alpha,R)+\sigma P_5(\alpha,R)}{P_1(\alpha,R)}$$
$$+2\gamma-4\gamma^2\frac{Z_2(\gamma,H)}{Z_1(\gamma,H)}+\frac{4\gamma}{1+\sigma}\frac{Z_3(\gamma,H)+\sigma Z_4(\gamma,H)}{Z_1(\gamma,H)}+\langle V_{\rm Coul}\rangle-V_e\left[1-\frac{P_7(\alpha,R)}{P_1(\alpha,R)}\right]\left[1-\frac{Z_5(\gamma,H)}{Z_1(\gamma,H)}\right]$$
$$-V_h\left[1-\frac{P_8(\alpha,R)}{P_1(\alpha,R)}\right]\left[1-\frac{Z_6(\gamma,H)}{Z_1(\gamma,H)}\right]\ , \tag{44}$$

which are new P_i-like (16) or Z_i-like (18) integrals with

$$\begin{aligned}
&F_7(\rho_e,\rho_h,\rho_{eh})=F_1(\rho_e,\rho_h,\rho_{eh})\theta(R-\rho_e)\ ,\\
&F_8(\rho_e,\rho_h,\rho_{eh})=F_1(\rho_e,\rho_h,\rho_{eh})\theta(R-\rho_h)\ ,\\
&G_5(z_e,z_h)=G_1(z_e,z_h)\theta(H/2-|z_e|)\ ,\\
&G_6(z_e,z_h)=G_1(z_e,z_h)\theta(H/2-|z_h|)\ .
\end{aligned} \tag{45}$$

The correlation energy is evaluated by subtracting from (44) the electron and the hole energy (40). See Fig. 9.

To study the influence of the confinement on the electron-hole distance, we define the transverse and axial mean quadratic distances r_{eh} and z_{eh}:

$$r_{eh}=(\langle\Psi_X|\rho_{eh}^2|\Psi_X\rangle/\langle\Psi_X|\Psi_X\rangle)^{1/2}\ , \tag{46}$$

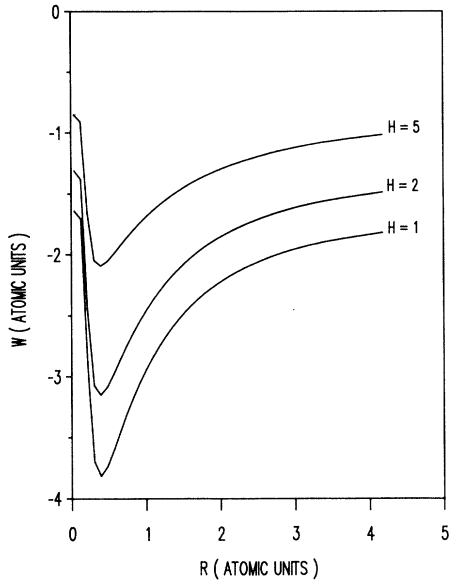

FIG. 9. Correlation energy (W) of an exciton in a cylinder, drawn against R for different values of H for $\sigma=0.196$ and $x=0.15$.

$$z_{eh}=[\langle\Psi_X|(z_e-z_h)^2|\Psi_X\rangle/\langle\Psi_X|\Psi_X\rangle]^{1/2}\ . \tag{47}$$

Figure 10 shows that the transverse electron-hole distance in the cylinder case has a minimal value near $0.5a_X^{3D}$ for $R\simeq 0.5a_X^{3D}$; this minimal value does not depend strongly on the value of H. Both for $R\rightarrow 0$ and $R\rightarrow\infty$, the 3D limit $\sqrt{2}a_X^{3D}$ must be obtained for large values of H, but our model fails when the ratio H/R becomes too large. The disk case is also reported. The 2D limit $\sqrt{3/8}a_X^{3D}=0.61a_X^{3D}$ is obtained for $R\rightarrow 0$ and $R\rightarrow\infty$. Figure 11 shows the behavior of the corresponding axial electron-hole distance.

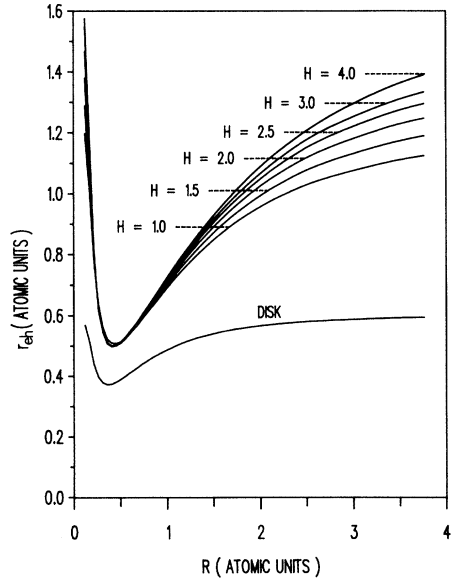

FIG. 10. Electron-hole in-plane distance r_{eh} (46), drawn against R for different values of H and in the disk model, for $\sigma=0.196$ and $x=0.15$.

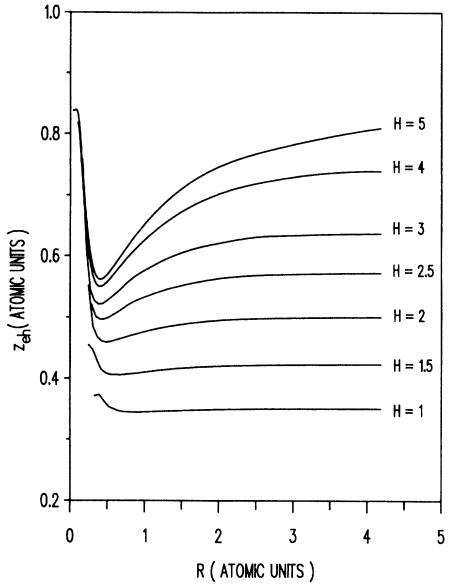

FIG. 11. Electron-hole axial distance z_{eh} (47), drawn against R for different values of H, for $\sigma=0.196$ and $x=0.15$.

V. CONCLUSION

A variational calculation has been performed to determine the influence of the shape and size of a cylindrical quantum dot on the binding energy of a confined electron-hole pair. The simpler case of infinite potential barriers has first been studied in order to check the validity of our wave function. In this case, it appears that, for small cylinder dimensions, the effect of the quantum confinement becomes predominant in comparison with that of the Coulombic interaction, in agreement with a previous study.[34] However, the latter, which has been performed by using a full correlated wave function, leads to better results at high H and R values. For very small dot sizes, the infinite-well model fails strongly because tunneling effects become very important. Indeed, the calculations performed with infinite band offsets show that the effect of the quantum confinement is no longer predominant at small cylinder sizes. In the case of the $GaAs/Ga_{1-x}Al_xAs$ system, it appears that the effect of the quantum confinement is the highest for dot dimensions near 50 Å.

ACKNOWLEDGMENTS

This work has been performed at the Centre de Calcul de Strasbourg Cronenbourg (CNRS). It was supported by the Centre National de la Recherche Scientifique and the Ministère de l'Education Nationale (DRED).

[1]L. Esaki, in *Physics and Applications of Quantum Wells and Superlattices,* Vol. 170 of *NATO Advanced Study Institute, Series B: Physics,* edited by E. E. Mendez and K. von Klitzing (Plenum, New York, 1987), p. 1.
[2]L. Brus, Appl. Phys. A **53**, 465 (1991).
[3]L. Brus, IEEE J. Quantum Electron. **22**, 1909 (1986).
[4]P. M. Petrof, A. C. Gossard, R. A. Logan, and W. Wiegmann, Appl. Phys. Lett. **41**, 635 (1982).
[5]J. Cibert, P. M. Petrof, G. J. Dolan, S. J. Pearton, A. C. Gossard, and J. H. English, Appl. Phys. Lett. **49**, 1275 (1986).
[6]K. Kash, A. Scherer, J. M. Worlock, H. G. Craighead, and M. C. Tamargo, Appl. Phys. Lett. **49**, 1043 (1986).
[7]M. A. Reed, R. T. Bate, K. Bradshaw, W. M. Duncan, W. R. Frensley, J. W. Lee, and H. D. Shih, J. Vac. Sci. Technol. B **4**, 358 (1986).
[8]J. Cibert, P. M. Petroff, G. J. Dolan, D. J. Werder, S. J. Pearton, A. C. Gossard, and J. H. English, Superlatt. Microstruct. **3**, 35 (1987).
[9]Y. Miyamoto, M. Cao, Y. Shingai, K. Furuya, Y. Suematsu, K. G. Ravikumar, and S. Arai, Jpn. J. Appl. Phys. **26**, L225 (1987).
[10]H. Temkin, G. J. Dolan, M. B. Panish, and S. N. G. Chu, Appl. Phys. Lett. **50**, 413 (1987).
[11]M. A. Reed, J. N. Randall, R. J. Aggarwal, R. J. Matyi, T. M. Moore, and A. E. Wetsel, Phys. Rev. Lett. **60**, 535 (1988).
[12]M. Watt, C. M. Sotomayor-Torres, R. Cheung, C. D. W. Wilkinson, H. E. G. Arnot, and S. P. Beaumont, J. Mod. Opt. **35**, 365 (1988).
[13]H. E. G. Arnot, M. Watt, C. M. Sotomayor-Torres, R. Glew, R. Cusco, J. Bates, and S. P. Beaumont, Superlatt. Microstruct. **5**, 459 (1989).
[14]Ch. Sikorski and U. Merkt, Phys. Rev. Lett. **62**, 2164 (1989).
[15]O. Brand, L. Tapfer, K. Ploog, R. Bierwolf, M. Hohenstein, F. Phillipp, H. Lage, and A. Heberle, Phys. Rev. B **44**, 8043 (1991).
[16]Al. L. Efros and A. L. Efros, Fiz. Tekh. Poluprovodn. **16**, 1209 (1982) [Sov. Phys. Semicond. **16**, 772 (1982)].
[17]L. E. Brus, J. Chem. Phys. **80**, 4403 (1984).
[18]A. I. Ekimov, A. A. Onushchenko, A. G. Plyukhin, and Al. L. Efros, Zh. Eksp. Teor. Fiz. **88**, 1490 (1985) [Sov. Phys. JETP **61**, 891 (1985)].
[19]Y. Kayanuma, Solid State Commun. **59**, 405 (1986).
[20]H. M. Schmidt and H. Weller, Chem. Phys. Lett. **129**, 615 (1986).
[21]S. V. Nair, S. Sinha, and K. C. Rustagi, Phys. Rev. B **35**, 4098 (1987).
[22]T. Takagahara, Phys. Rev. **36**, 9293 (1987).
[23]Y. Kayanuma, Phys. Rev. B **38**, 9797 (1988).
[24]E. J. Austin, Semicond. Sci. Technol. **3**, 960 (1988).
[25]J. B. Xia, Phys. Rev. B **40**, 8500 (1989).
[26]G. B. Grigoryan, A. V. Rodina, and Al. L. Efros, Fiz. Tverd. Tela (Leningrad) **32**, 3512 (1990) [Sov. Phys. Solid State **32**, 2037 (1990)].
[27]Y. Kayanuma and H. Momiji, Phys. Rev. B **41**, 10 261 (1990).
[28]D. B. T. Thoai, Y. Z. Hu, and S. W. Koch, Phys. Rev. B **42**, 11 261 (1990).
[29]C. F. Lo and R. Sollie, Solid State Commun. **79**, 775 (1991).
[30]S. I. Pokutnil, Fiz. Tekh. Poluprovodn. **25**, 628 (1991) [Sov. Phys. Semicond. **25**, 381 (1991)].
[31]G. T. Einevoll, Phys. Rev. B **45**, 3410 (1992).
[32]G. W. Bryant, Phys. Rev. Lett. **59**, 1140 (1987).
[33]G. W. Bryant, Phys. Rev. B **37**, 8763 (1988).
[34]Y. Kayanuma, Phys. Rev. B **44**, 13 085 (1991).
[35]*Handbook of Mathematical Functions,* edited by M. Abramowitz and I. A. Stegun (Dover, New York, 1972).
[36]R. C. Miller, D. A. Kleinman, and A. C. Gossard, Phys. Rev. B **29**, 7085 (1984).
[37]H. J. Lee, L. Y. Juravel, J. C. Wolley, and A. C. Springthorpe, Phys. Rev. B **21**, 659 (1980).
[38]R. L. Greene and K. K. Bajaj, Solid State Commun. **45**, 825 (1983).